O−H Stretch Overtone Excitation in Methyl and Ethyl Hydroperoxides

Sarah C. Homitsky, Sonia M. Dragulin,† Laura M. Haynes, and Shizuka Hsieh*

Chemistry Department, Smith College, Clark Science Center, Northampton, Massachusetts 01063

Received: June 12, 2004; In Final Form: August 20, 2004

We use laser photoacoustic spectroscopy to obtain vibrational overtone spectra in the regions of four and five quanta of O−H stretch ($4\nu_{OH}$ and $5\nu_{OH}$) for gas-phase methyl (MeOOH), ethyl (EtOOH), and *tert*-butyl hydroperoxide (*t*-BuOOH). Integrated cross sections for the main peak due to O−H stretch excitation to $4\nu_{OH}$ are similar for all three hydroperoxides ($\sim 2 \times 10^{-21}$ cm^2 molecule^{-1} cm^{-1}); cross sections for excitation to and $5\nu_{OH}$ are an order of magnitude smaller. Interpretation of spectral features using a previously reported vibration−torsion model for ROOH molecules, where excitation of torsional motion about the O−O bond accompanies vibrational excitation, yields plausible fits to the spectra. Simulations with the vibration−torsion model and ab initio calculations suggest barriers for torsional motion about the O−O bond to be higher in *t*-BuOOH than in MeOOH and EtOOH, with a trend of increasing trans torsional barrier height with increasing size of the R group.

1. Introduction

Two applications of overtone excitation and spectroscopy provide the motivation for this work. The first is the role of overtone excitation in the atmospheric formation of hydroxyl radicals (OH) via a mechanism called direct overtone photolysis.[1,2] Like hydrogen peroxide (HOOH), methyl hydroperoxide (MeOOH) is a source of HO_x free radicals in the upper troposphere,[3] but its overtone excitation has not yet been investigated and its cross section is unknown. The second application is the determination of barriers to torsional motion about the O−O bond in hydroperoxides. Crim and co-workers attribute features in *tert*-butyl hydroperoxide (*t*-BuOOH)[4] and HOOH[5] overtone spectra to torsional excitation about the O−O bond. They obtain from the spectra experimental values for the trans torsional barrier in the ground and vibrationally excited molecules.

1.1. Overtone Excitation in Atmospheric Chemistry. Recent work implicates direct overtone photolysis of atmospheric species as a source of OH radicals.[1,2,6] The direct overtone photolysis mechanism involves absorption of near-infrared or visible light to excite several quanta of vibration followed by unimolecular dissociation. Quantifying the contribution of the direct overtone photolysis mechanism to OH formation in the atmosphere by modeling requires reliable predictions of dissociation lifetimes and absorption cross sections. Using estimated collisional deactivation time scales and absorption cross sections, for example, Donaldson et al. report theoretical values for the contributions to atmospheric OH from the direct overtone photolysis of nitric acid ($HONO_2$), peroxynitric acid (HO_2NO_2), and HOOH.[1] While the process is significant for molecules with weak O−O bonds (bond strength 95.3 kJ mol^{-1} for HO_2NO_2),[6] direct overtone photolysis for hydroperoxides typically requires five or more quanta of O−H stretch excitation in order to break the O−O bond (bond strength ∼188 kJ mol^{-1} [7]).

Similar to HOOH,[8] the molecules addressed in this work (MeOOH, EtOOH, and *t*-BuOOH) can undergo direct overtone photolysis where overtone excitation of the O−H stretch results in cleavage of the O−O bond and OH radical formation. The groups of Crim[9] and of Zare[10,11] have characterized the direct overtone dissociation of *t*-BuOOH from the $5\nu_{OH}$ and $6\nu_{OH}$ states both experimentally and theoretically. While the direct overtone photolysis of MeOOH or EtOOH has not been observed, a theoretical study[12] of MeOOH suggests that it has enough energy to dissociate from states excited with six or more quanta of O−H stretch ($\geq 6\nu_{OH}$) and that its dissociation rate is more similar to that of HOOH than to that of *t*-BuOOH. Because its predicted dissociation rate is relatively fast, direct overtone photolysis, as opposed to collisional deactivation, can be considered a probable fate for highly vibrationally excited MeOOH, and perhaps also EtOOH. As the process of overtone-initiated decomposition only contributes a 2% enhancement to the atmospheric photolysis rate of HOOH,[13] however, any contribution to atmospheric OH from the overtone excitation of MeOOH and EtOOH is likely to be very small. Still, the importance of cross section measurements to atmospheric chemistry prompts us to make crude measurements of cross sections using photoacoustic spectroscopy.

1.2. Torsional Barriers for Motion about the O−O Bond. Crim and co-workers use a vibration−torsion spectroscopic model to interpret spectral features in HOOH[5] and *t*-BuOOH[4] O−H stretch overtone spectra. They assign the main band to O−H stretch excitation and the smaller peak at higher energy to O−H stretch excitation accompanied by one quantum of torsional excitation for motion about the O−O bond. For *t*-BuOOH the model yields trans torsional barrier heights in the ground and vibrationally excited states ($4\nu_{OH}$, $5\nu_{OH}$, and $6\nu_{OH}$). They find the trans barrier for *t*-BuOOH to be 275 ± 25 cm^{-1} in the ground vibrational state and to have increasing values with increasing O−H stretch excitation, a trend they also observe for HOOH.[5]

While the torsional barrier for *t*-BuOOH in its vibrational ground state has not been determined by other methods, those in HOOH and MeOOH have been studied both experimentally

* Address correspondence to this author. Phone: (413) 585-4495. Fax: (413) 585-3786. E-mail: shsieh@email.smith.edu.

† Present address: Department of Chemistry, University of Wisconsin, Madison, Wisconsin 53706.

10.1021/jp047455l CCC: $27.50 © 2004 American Chemical Society
Published on Web 10/12/2004

and computationally.[14] Experimental[15] values reported for HOOH in its vibrational ground state are 387 cm^{-1} for the trans barrier and 2563 cm^{-1} for the cis barrier. Analysis of microwave spectra yields a trans barrier height of 172.5 cm^{-1} for MeOOH,[16] and electronic structure calculations reproduce the experimental value to within ∼30 cm^{-1}, with a best theoretical value of 132 ± 10 cm^{-1}.[14] Tonmunphean et al. also calculate the cis barrier to be 2010 ± 10 cm^{-1}.[14]

The heights of the barriers to torsional motion have implications on the interpretation of results from photodissociation experiments of the ROOH molecules, as increased torsional motion in a parent ROOH molecule causes alignment of the OH fragment angular momentum (J) with its recoil velocity vector (v).[17] In their interpretation of the ultraviolet photodissociation of *t*-BuOOH,[17] Brouard[18] and co-workers assume it to have a low torsional barrier (∼80 cm^{-1}). They find that the expected wide-motion torsional excitation, however, only becomes important for fragments produced with high J values. A report of the photodissociation of cumene hydroperoxide[19] attributes the observed positive $v-J$ correlation in OH fragments to a torsional barrier much lower than the zero-point energy.

The apparent conflict between the assumption of a low (∼80 cm^{-1}) trans barrier in *t*-BuOOH and the value predicted by Likar et al.[4] (275 ± 25 cm^{-1}) prompts us to calculate the trans barrier. We also apply the vibration−torsion model to our spectra of MeOOH and EtOOH. For all three hydroperoxides the vibration−torsion analysis is consistent with calculated trans barrier heights, leading to the conclusion of a lower trans barrier height for O−O torsion in MeOOH and EtOOH versus *t*-BuOOH. The calculations support the work of Likar et al.[4]

2. Experimental Photacoustic Spectra

2.1. Photoacoustic Setup. Doubled light from a Nd:YAG laser (Spectra Physics LAB150, 10-ns pulses at 10 Hz) pumps a dye laser (Sirah Cobra Stretch) to generate visible light with 0.05-cm^{-1} resolution. The dyes used are LDS 751 and a mixture of Rhodamine 610 and 640 in methanol. After a series of turning prisms the light enters a glass cell (2.5-cm diameter, 35-cm length) with removable windows at Brewster's angle and a microphone (Knowles EK-3132) positioned near the center of the cell (∼1.5 cm off the laser beam path). We monitor the amplified microphone signal (boxed and integrated with a Stanford Research Systems 250 Boxcar Integrator) as a function of laser wavelength to collect photoacoustic spectra. Laser pulse energies measured at the gas cell range from 5 to 40 mJ, and a thermopile power meter (Ophir AP-10) at the output end of the cell monitors the laser power. We have verified the signal's linear dependence on laser power and normalize spectra for variations in power.

2.2. Sample Preparation and Handling. The samples consist of vapor from aqueous hydroperoxide (ROOH) solutions. Bubbling argon through the aqueous sample solution and flowing the gas mixture through the cell to maintain a constant pressure in the range of 80−100 Torr maximizes the signal and makes it more robust to slight changes (<2 Torr) in sample pressure. Aqueous solutions of HOOH (30% or 50%) and *t*-BuOOH (70%) are from Aldrich. We use samples as purchased, after a freeze−pump−thaw cycle, and assume the concentrations to match those reported by the manufacturer. Since MeOOH and EtOOH are not commercially available, we follow a procedure for preparing aqueous MeOOH and EtOOH that minimizes the HOOH in the reaction mixture.[20]

Reagents for the synthesis of MeOOH and EtOOH are from Aldrich and Fisher Scientific. Hydrogen peroxide solution (30%, 5 mL), distilled water (14 mL), and dimethyl sulfate or diethyl sulfate (5.5 mL) are combined in a three-neck, 1000-mL round-bottom flask placed in an ice bath. The flask is equipped with magnetic stirring and fitted with a condensor, thermometer, and dropping funnel. Potassium hydroxide solution (40%, 11.6 mL) is added dropwise to the reaction mixture. After the addition of the potassium hydroxide solution, the reaction mixture is heated gently until bubbles cease to appear.[21] The reaction mixture is allowed to reach room temperature. Aliquots are taken from the reaction flask to determine the peroxide concentrations as described below.[20,22] Before use, the reaction mixture is neutralized with 50% sulfuric acid at 273 K.

We analyze aliquots from the reaction mixture to determine MeOOH or EtOOH concentration. The analysis follows the approach of Davies and Deary[20] that assumes the MeOOH or EtOOH concentration to be the difference between the total peroxide concentration and the contribution from HOOH. Several hours after the synthesis procedure, the MeOOH and EtOOH solutions no longer show indications of HOOH.[20] The assays for total peroxides and HOOH are as follows. For the total peroxide concentration, we use the method of Behrman et al.[23] Sulfuric acid (2 M, 20 mL), water (4.5 mL), and aqueous potassium iodide (1 g in 10 mL) are added to each aliquot of the reaction mixture (0.5 mL). After the mixtures sit in the dark for 60 min, samples (5 mL) are taken and titrated with sodium thiosulfate solution (0.01 M).[23] We have tested the titration assay using the HOOH and *t*-BuOOH solutions from Aldrich, and results are consistent with their reported concentrations. The assay for HOOH concentration is a spectrophotometric method similar to that of Sellers.[24] A calibration curve is constructed for absorbance against a blank at 400 nm (Varian Cary 50 Bio UV−visible spectrophotometer). To prepare the samples HOOH solutions (reaction mixture or 0.00445 M HOOH standard) are added to sulfuric acid (2 M, 3 mL) and titanium(IV) oxysulfate (15 wt % solution in dilute sulfuric acid, 0.5 mL) and diluted to a total volume of 50 mL with deionized water.

2.3. Estimating Absorption Cross Sections. Previous absorption cross section measurements of gas-phase samples with photoacoustic spectroscopy involve comparison of signal intensity with that of a molecule of known cross section, usually methane.[25] Here we rely upon known cross sections of water vapor (HITRAN database[26]) to estimate cross sections of the gas-phase hydroperoxides (ROOH). Since the vapor from the aqueous samples contains both water and ROOH, we monitor the relative magnitude of signals in a narrow wavelength region where water absorbs (typically 729.45−729.05 or 629.40−629.95 nm) and over the top of the main ROOH peak. To capture the sharp peaks from water, its spectra are taken with smaller step sizes (<0.001 nm) than the ROOH spectra (0.05 nm). We normalize hydroperoxide spectra to the intensity of the main ROOH peak. Assuming that the integrated signal (S) under each peak is directly proportional to both the integrated absorption cross section (σ) and the partial pressure (P) of the absorber, the ratio of the water and ROOH peak areas yields the hydroperoxide integrated cross section (σ_{ROOH}), as long as the relative partial pressures and water vapor cross section are known. We determine the hydroperoxide cross section using the following relationship.

$$\frac{S_{ROOH}}{S_{H_2O}} = \frac{P_{ROOH}\sigma_{ROOH}}{P_{H_2O}\sigma_{H_2O}}$$

The simple strategy outlined above for determining hydroperoxide cross sections (σ_{ROOH}) from relative signals of water

TABLE 1: Estimated Partial Pressures above Aqueous Solutions at 295 K

	soln concn (M)	ROOH partial pressure (Torr)	H_2O partial pressure (Torr)
HOOH	9.8	0.13[a]	14.7[a]
t-BuOOH	7.0	6.5[b]	13.5[b]
	0.10	0.16[c]	19.8
	0.05	0.08[c]	19.8
MeOOH	0.40	0.81[d]	19.8
EtOOH	0.70	1.3[d]	19.8

[a] Extrapolated from Tables 17 and 18 in Chapter 5 of ref 28. [b] Estimated assuming Raoult's law and a total vapor pressure of 20 Torr at 295 K. [c] Estimated assuming a Henry's law constant (K_H) of 465 M atm^{-1} that we determined from analyzing the vapor condensate from a 0.1 M solution. [d] Based on Henry's law constants from ref 30.

and hydroperoxide is only reliable if three basic assumptions hold true. The first assumption is that the instrument response is independent of the identity of the absorber. Included in this assumption is the approximation that the efficiency of collisional energy transfer is the same for all absorbers. The second assumption is that the signal magnitude is directly proportional to the concentration of the absorber. The observed linear signal response of signal to partial pressure of the absorber (not shown) supports this second assumption. The third assumption is that the vapor composition is known; we assume the vapor pressure above the sample to reflect the predicted equilibrium vapor composition. Since partial vapor pressures above solutions are not known exactly for MeOOH, EtOOH, and *t*-BuOOH, we make approximations, as described in more detail below. This third assumption is the weakest point in our estimation of absorption cross sections for the hydroperoxides, not only because of the estimated partial pressures (Table 1) but also because of the interaction of the gases with the cell wall. As pointed out by Gutow et al.,[25] the tendency of water vapor to stick to glass walls complicates knowing the vapor composition with certainty. Since the hydroperoxides also stick to the walls, we make the assumption that the sticking tendencies of the different molecules are comparable. An observed increase in signal with increasing sample concentration supports the overall assumption qualitatively. Analysis of the condensate of the gas that passes through the cell supports the assumption quantitatively within 10%.

We base estimated vapor concentrations (Table 1) on concentrations of peroxides in solution, as reported by Aldrich (for the cases of HOOH and *t*-BuOOH) or as determined using the methods described in Section 2.2 (for MeOOH and EtOOH). For MeOOH and EtOOH, evidence for peroxide decomposition in solution further complicates the measurements.[27] From the observed decrease in hydroperoxide signal with time and from assays of the sample solution before and after an experimental run, we estimate a drop of 20−30% in MeOOH or EtOOH concentration over a period of 90 min.[27] We did not notice peroxide decomposition for the cases of HOOH and *t*-BuOOH. To minimize the effects of peroxide decomposition for all four molecules, we alternate between measurements of the peroxide and water as quickly as possible, making scans in small sections of each region. Typical scan times are under 15 min so that both water and peroxide regions are recorded within at least 30 min. Given our estimated rate of peroxide decomposition, the effect contributes uncertainty no greater than the reported standard deviations (Table 2) that reflect our experimental reproducibility.

HOOH provides a test case for our methods and assumptions. Using the known[28] values of equilibrium vapor pressures for aqueous solutions of HOOH, we estimate a cross section value for the main $4\nu_{OH}$ peak that is within error of a superior measurement using cavity ring-down spectroscopy[13] (Table 2). Since vapor pressure compositions are not known exactly for the ROOH solutions, we approximate them using Raoult's or Henry's law and solution concentrations determined as described above (Table 1). For MeOOH and EtOOH we use reported Henry's law constants,[29,30] but for *t*-BuOOH we use a value based on analysis of the vapor condensate. Using Henry's law with solutions of low concentration (0.05 and 0.1 M) or Raoult's law with high concentrations (7 M) yields similar results for *t*-BuOOH, so we consider our assumptions adequate for the final cross section values for *t*-BuOOH (Table 2). Our values are about four times larger than cross sections from a previous work for *t*-BuOOH at $5\nu_{OH}$, but subsequent authors indicate a 50% uncertainty in their absolute measurements.[10,11] The MeOOH and EtOOH cross sections (Table 2) carry more systematic uncertainty since solution impurities are likely to shift the vapor composition away from that predicted by Henry's law. The low vapor concentrations for MeOOH and EtOOH (Table 1) result in a lower signal-to-noise ratio and therefore higher standard deviations in the reported values (Table 2). Figure 1 shows spectra with our best determination of cross sections.

TABLE 2: Integrated Cross Sections (cm^2 molecule^{-1} cm^{-1}) for the Main Peak for the O−H Stretch Overtone

	$4\nu_{OH}$	$5\nu_{OH}$
HOOH[b]	$(6.1 \pm 1.1) \times 10^{-21}$	
HOOH[a]	$(4.58 \pm 0.39) \times 10^{-21}$	$(5.67 \pm 0.52) \times 10^{-22}$
MeOOH[b,c]	$(2.7 \pm 0.3) \times 10^{-21}$	$(2.1 \pm 1.3) \times 10^{-22}$
EtOOH[b,c]	$(1.6 \pm 0.6) \times 10^{-21}$	$(1.9 \pm 1.6) \times 10^{-22}$
t-BuOOH[b,c]	$(1.7 \pm 0.4) \times 10^{-21}$	$(1.7 \pm 0.5) \times 10^{-22}$

[a] From ref 13. [b] Uncertainties reported are standard deviations from three or more trial runs and do not take into account any differences in vapor composition from those reported in Table 1. [c] Integrated intensities are for the main peak, which encompasses transitions involving no change in torsional level (illustrated in Figure 2 as S_0^0, A_0^0, S_1^1, and A_1^1).

3. Barriers to Torsion about the O−O Bond

3.1. Qualitative Trends. The vibration−torsion spectroscopic model of Crim and co-workers[5] accounts for the coarse features in the spectra. To describe these features we follow their notation for denoting transitions. Likar et al. use S_i^j and A_i^j to indicate transitions between S or A symmetry states from torsional level i in the ground vibrational state ($0\nu_{OH}$) to torsional level j in the vibrationally excited state ($4\nu_{OH}$ or $5\nu_{OH}$).[4] In the model the main peak corresponds to a vibrational transition without any torsional excitation (S_0^0 and A_0^0, Figure 2). The smaller peak at higher photon energy corresponds to a hot band involving torsional excitation (S_1^1 and A_1^1), and the peak at even higher energy corresponds to a combination of vibrational and torsional excitation (S_0^1 and A_0^1). We interpret the additional feature at low photon energy in the MeOOH $4\nu_{OH}$ (Figure 3) to a hot band transition from a torsionally excited state to a vibrationally excited state without torsional excitation (S_1^0 and A_1^0).

Because the model predicts that the energy differences between spectral features are directly related to the energy spacings between torsional energy levels in the ground and vibrationally excited states (Figure 2), trends in the spectra lead to two predictions. The first is an increase in torsional energy level spacing with increasing vibrational excitation, as Crim and co-workers have observed previously for HOOH[5] and

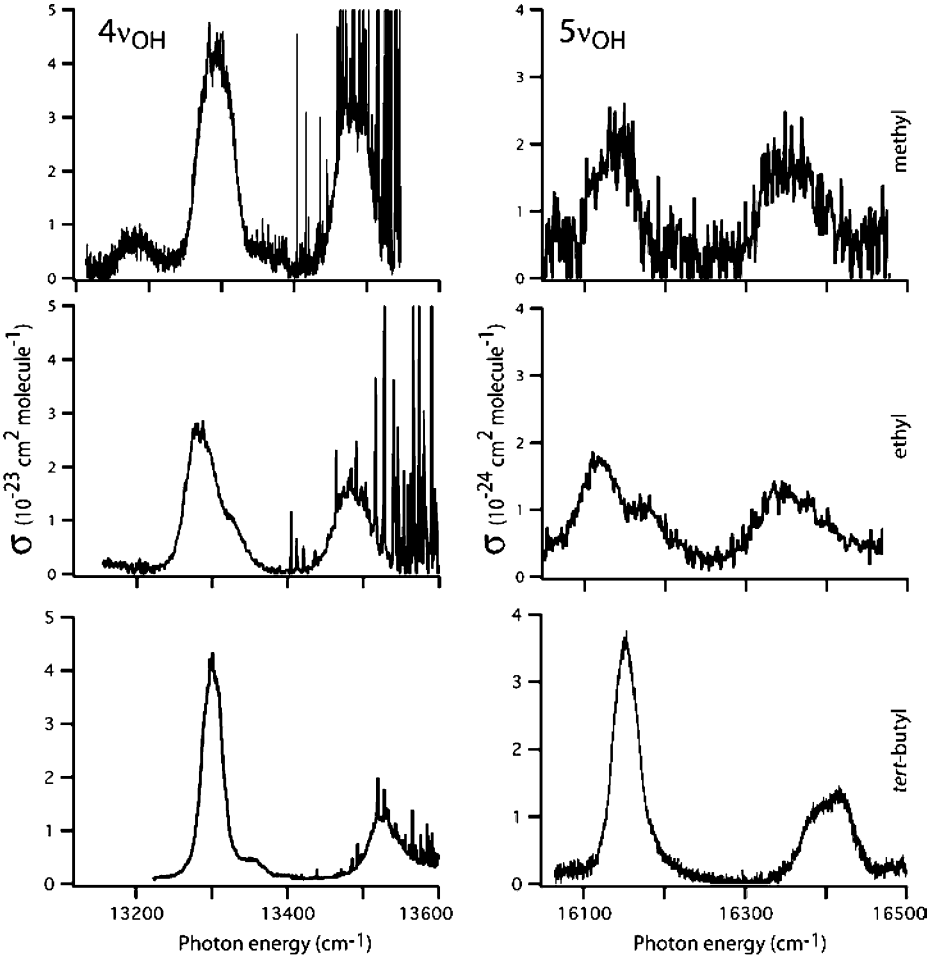

Figure 1. Photoacoustic spectra for hydroperoxides (ROOH) in the region of $4\nu_{OH}$ (left) and $5\nu_{OH}$ (right). Sharp lines around 13 500 cm^{-1} and higher are due to water. The low vapor pressures of MeOOH and EtOOH (Table 1) lower the signal magnitude and therefore also the signal-to-noise ratio. Standard deviations in cross section determinations for the main peaks, which are unhampered by water lines, are listed in Table 2.

t-BuOOH.[4] The second is an increase in torsional energy level spacing with increasing size of the R group within the series studied here (Figure 3). Since the model shows the torsional energy level spacing to be most sensitive to the trans barrier height (V_{trans}) for torsion about the O−O bond,[4] the second trend indicates an increase in V_{trans} with increasing size of the R group. Calculations (Figure 4) and the model's quantitative treatment, described below, support the simple qualitative prediction.

3.2. Vibration−Torsion Spectroscopic Model. The vibration−torsion model assumes the O−H stretch vibration and the torsional motion about the O−O to be adiabatically separate so that simulating the positions of peaks in the spectra involves solving for the torsional states that accompany a given vibrational state. We use a program rewritten in Mathcad but based on code originally written by Dübal and Crim in FORTRAN. Given initial input parameters for describing the kinetic energy and potential energy operators, the program solves the Schrödinger equation for torsional motion. Energy levels in the ground and excited vibrational states are taken as the sum of vibrational energy and torsional excitation energy.

For defining the Hamiltonian,[5] the potential (Figure 5) as a function of torsional angle (R−O−O−H dihedral angle, χ) is described by

$$V(\chi) = \sum_{i=0}^{3} V_i \cos i\chi$$

and the kinetic energy operator is

$$\hat{E}_K = -\frac{d}{d\chi}\alpha(\chi)\frac{d}{d\chi}$$

where

$$\alpha(\chi) = \alpha_0 + \alpha_1 \cos\chi$$

The parameters for potential energy (V_0, V_1, V_2, and V_3) can be expressed in terms of the cis and trans barrier heights, and the kinetic energy parameters (α_0 and α_1) are a function of molecular geometry and masses, as described in detail in the Appendix of Likar et al.[4] Solutions are found in basis sets of $\sin n\chi$, $\sin(n + {}^1/_2)\chi$, $\cos n\chi$, and $\cos(n + {}^1/_2)\chi$, with $n = 0$ to 19, resulting in states with the labels *ea*, *oa*, *es*, and *os*, respectively.[5] Likar et al.[4] group the *ea* and *oa* states, which are antisymmetric about $\chi = 180°$, as A states and the *es* and *os* states, which are symmetric about $\chi = 180°$, as S states. Transitions are limited between states of the same symmetry.[4]

Unlike more sophisticated calculations[31−33] for predicting overtone absorption cross sections, the model does not take into account the dependence of the dipole moment function on dihedral angle for predicting relative peak intensities. The relative peak intensities shown here are based only on Franck−Condon factors and room-temperature populations. Calculations of absolute overtone absorption cross sections that take into

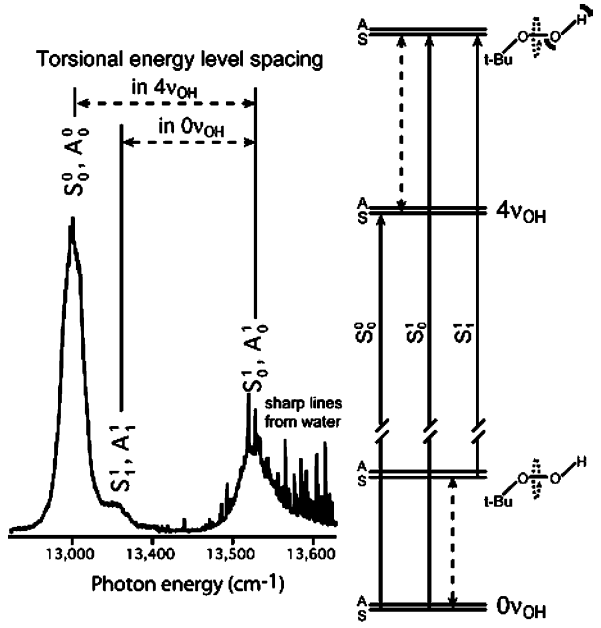

Figure 2. Peak assignments in the $4\nu_{OH}$ region for *tert*-butyl hydroperoxide from Crim and co-workers. Spacings between peaks, shown above the spectrum, directly reflect torsional energy level spacings in the ground ($0\nu_{OH}$) and excited ($4\nu_{OH}$) vibrational states, illustrated on the energy level diagram to the right. Assignments are from Likar et al.,[4] who also indicate that the structure around 13 530 cm^{-1} contains a contribution from *tert*-butyl alcohol. The notation S_i^j or A_i^j indicates transitions between S or A symmetry states from a torsional level of *i* in the ground vibrational state to a level of *j* in the vibrationally excited state. See Section 3.2 for a brief description of the torsional states (A, S) or refs 4 and 5 for more detail.

TABLE 3: ROOH Equilibrium Geometries[a]

	R_{OO}	R_{OH}	R_{OC}	∠OOH	∠OOR	χ_{ROOH}
MeOOH[b]	1.4505	0.9655	1.4140	100.6	106.6	116.3
MeOOH[c]	1.449	0.966	1.41	100.8	106.8	115
EtOOH[c]	1.449	0.966	1.43	100.8	108.8	113
t-BuOOH[c]	1.449	0.965	1.45	100.8	109.8	113
t-BuOOH[d]	1.475	0.959	1.4	94.8	94.8	118

[a] Bond lengths in Å and angles in deg. [b] Calculations by Tonmunphean et al. (ref 14) with B3LYP and the cc-pVQZ basis set. [c] Values used in this work from B3LYP calculations with the 6-311++G(3df,2pd) basis set. [d] Values used by Likar et al.[4] for input into their vibration−torsion model.

account the dipole moment function dependence on torsional angle are underway and will be presented in a future work. The simulations here are only meant to account for crude features and to relate the trends in the spectra to trans barrier heights.

3.3. Input Parameters. The vibration−torsion model requires equilibrium geometries for determining the kinetic energy parameters (α_0 and α_1) and torsional barrier heights (V_{cis} and V_{trans}) for describing the torsional potential (Tables 3 and 4). Gaussian 98[34] provides parameters for the ground vibrational state geometries (Table 3). Changes in V_{cis} as high as ±200 cm^{-1} produce little difference in the calculated energy levels and in the visual appearance of the final spectrum. For V_{cis} values, therefore, we use values determined from calculations in a manner similar to that shown in Figure 5 without any adjustments. While the simulations are relatively insensitive to changes in V_{cis} values, the appearance of the simulated spectra changes significantly with the input value of V_{trans}.[4] Changing the value of V_{trans} beyond ±25 cm^{-1} causes visually noticeable changes in the spacing between spectral peaks in the simulations. Because the model is sensitive to relatively small changes in the input value of V_{trans}, we leave it as an adjustable parameter for fitting the experimental spectra.

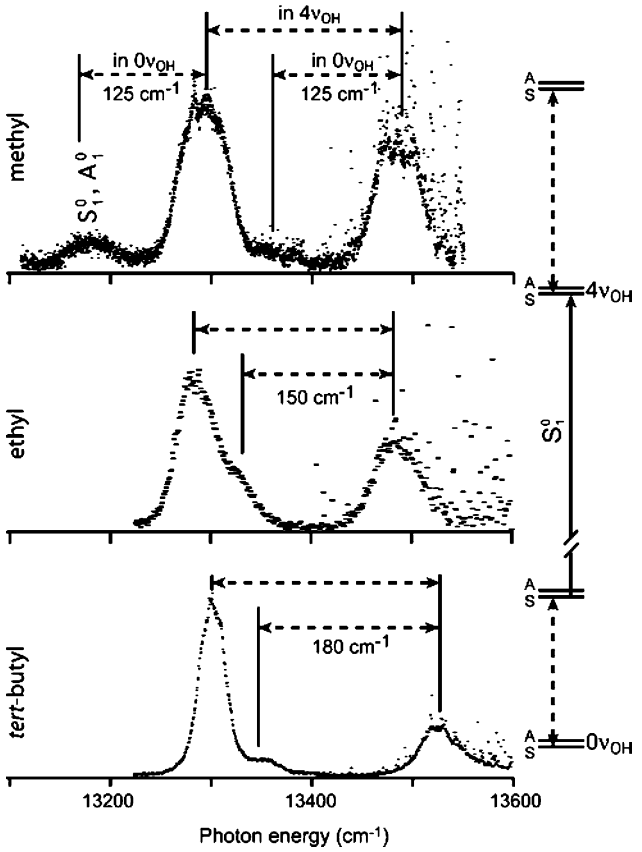

Figure 3. Torsional energy level spacing as a function of hydroperoxide (ROOH) R group. The $4\nu_{OH}$ spectrum for MeOOH (top) shows a hot band at low energy. Spacings between peaks are labeled to illustrate a trend of increasing torsional energy level spacing with R group size for the molecules in their ground vibrational states. Section 3.4 describes the direct relationship between the trend shown here and the trend of increasing torsional barrier with R group size shown in Figure 4.

Likar et al.[4] provide guidance for selecting parameters for the vibrationally excited states. We adopt their assumption that the excited-state geometry is identical to the ground-state geometry with the exception of an extended O−H bond length and compressed dihedral angle. For the determination of kinetic energy parameters (α_0 and α_1), we use ground-state bond lengths and angles (Table 3) with values for extended O−H bond lengths from Likar et al. (1.041 and 1.065 Å for $4\nu_{OH}$ and $5\nu_{OH}$, respectively).[4] Similarly for the dihedral angle in the vibrationally excited states, we use their value of 106°.[4] Given the relative insensitivity of simulations with respect to V_{cis}, we assume the same differences due to vibrational excitation as those observed for HOOH.[5] As in the vibrational ground-state case, we leave V_{trans} as an adjustable parameter.

3.4. Trans Torsional Barrier Heights. The V_{trans} values reported in Table 4 and displayed in Figure 4 are selected to match the energy differences between peaks in the experimental spectra. Since the energy difference between the combination band (S_0^1 and A_0^1) and the hot band (S_1^1 and A_1^1) directly reflects the energy spacing between torsional levels in the ground vibrational state, we consider reasonable V_{trans} values (Table 4) to be those yielding spacings of 125, 150, and 180 cm^{-1} for MeOOH, EtOOH, and *t*-BuOOH, respectively (Figure 4), within ±15 cm^{-1}. The spacing between the hot band at low energy (S_1^0 and A_1^0) and the main peak (S_0^0 and A_0^0), only observed for

TABLE 4: Input Parameters for the Vibration−Torsion Model

	ν_{OH}	V_{cis} (cm^{-1})	V_{trans} (cm^{-1})	χ (deg)	α_0 (cm^{-1})	α_1 (cm^{-1})	bandcenter (cm^{-1})
MeOOH	0	2100	130	116	21.70	0.613	
	4	2220	320	106	18.92	0.592	13267 ± 5
	5	2295	370	106	18.15	0.586	16110 ± 10
EtOOH	0	2000	185	113	21.42	0.627	
	4	2120	350	106	18.64	0.606	13257 ± 5
	5	2195	480	106	17.87	0.600	16083 ± 10
t-BuOOH	0	2400	275	113	21.16	0.633	
	4	2520	425	106	18.36	0.612	13296 ± 5
	5	2595	575	106	17.60	0.606	16130 ± 10
t-BuOOH[a]	0	2640	275 ± 25	118	20.39	0.225	
	4	2760	425 ± 50	106	17.44	0.215	
	5	2835	575 ± 60	106	16.68	0.213	

[a] Parameters used in the original application of the vibration−torsion model to *t*-BuOOH (ref 4).

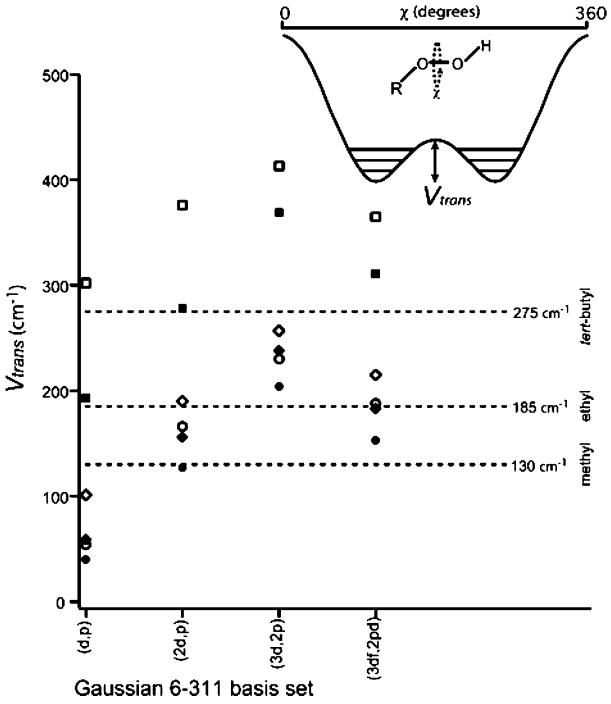

Figure 4. Calculated trans potential barrier heights (V_{trans}) for *t*-BuOOH (squares), EtOOH (diamonds), and MeOOH (circles). Calculations use B3LYP with standard basis sets ranging from 6-311G(d,p) to 6-311++G(3df,2pd). Solid shapes are for calculations including diffuse functions on hydrogens (++). The values reflect the energy difference between the fully optimized, energy-minimum structure and the optimized structure with a trans or cis configuration, as determined by the fixed dihedral angle (180° for trans or 0° for cis). We did not use transition state optimization options in the calculations. Dotted lines mark experimental values determined from photoacoustic spectra with the vibration−torsion model.

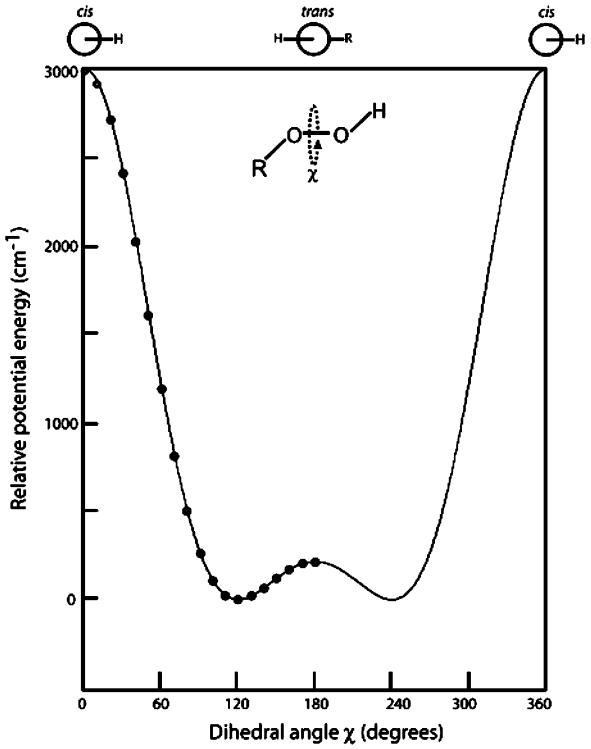

Figure 5. Shape of the potential for torsion about the O−O bond in *t*-BuOOH. Circles are points from calculations at the HF level with a 6-31+G(d,p) basis set, with geometry re-optimization in the remaining degrees of freedom at each value of χ. Energies do not include zero-point vibrational energies. The line is the potential function used in the vibration−torsion model drawn for the specific case of a 3000 cm^{-1} cis barrier and a 215 cm^{-1} trans barrier.

MeOOH at $4\nu_{OH}$, also implies a torsional energy level spacing of ~125 cm^{-1} for MeOOH in its ground vibrational state. To determine input V_{trans} values for the vibrationally excited states we depend similarly on the experimental energy difference between the combination band (S_0^1 and A_0^1) and the main peak (S_0^0 and A_0^0). Simple stick spectrum simulations from the vibration−torsion model using the input parameters listed in Tables 3 and 4 appear in Figure 6.

4. Discussion

4.1. Integrated Cross Sections. The measured cross sections (Table 2) have large standard deviations, reflecting our poor experimental reproducibility, but the values have reasonable magnitudes within expectations. It is anticipated that cross sections should decrease by an order of magnitude for an increase in the number of quanta of vibration excited,[35] and the rule of thumb roughly applies for each ROOH at $4\nu_{OH}$ and $5\nu_{OH}$. Refining the absorption cross section for MeOOH at $5\nu_{OH}$, where signal-to-noise levels are currently low, and obtaining a value at $6\nu_{OH}$ are of continued interest to our lab since direct overtone dissociation to form OH probably occurs from these states. Ongoing calculations for the absolute absorption cross sections will supplement future experimental work.

4.2. Torsional Barrier Heights. Of the hydroperoxide series, MeOOH has the lowest trans barrier to motion about the O−O bond. Using the vibration−torsion model and experimental spectra (Figure 3) we estimate $V_{trans} \approx 130$ cm^{-1}, which is in close agreement with a previously calculated value (132 cm^{-1} [14]) but farther from the experimental value from microwave spectroscopy (172.5 cm^{-1} [16]). Using the earlier experimental value ($V_{trans} = 172.5$ cm^{-1} [16]) in the vibration−torsion model results in a predicted torsional energy level spacing that is high

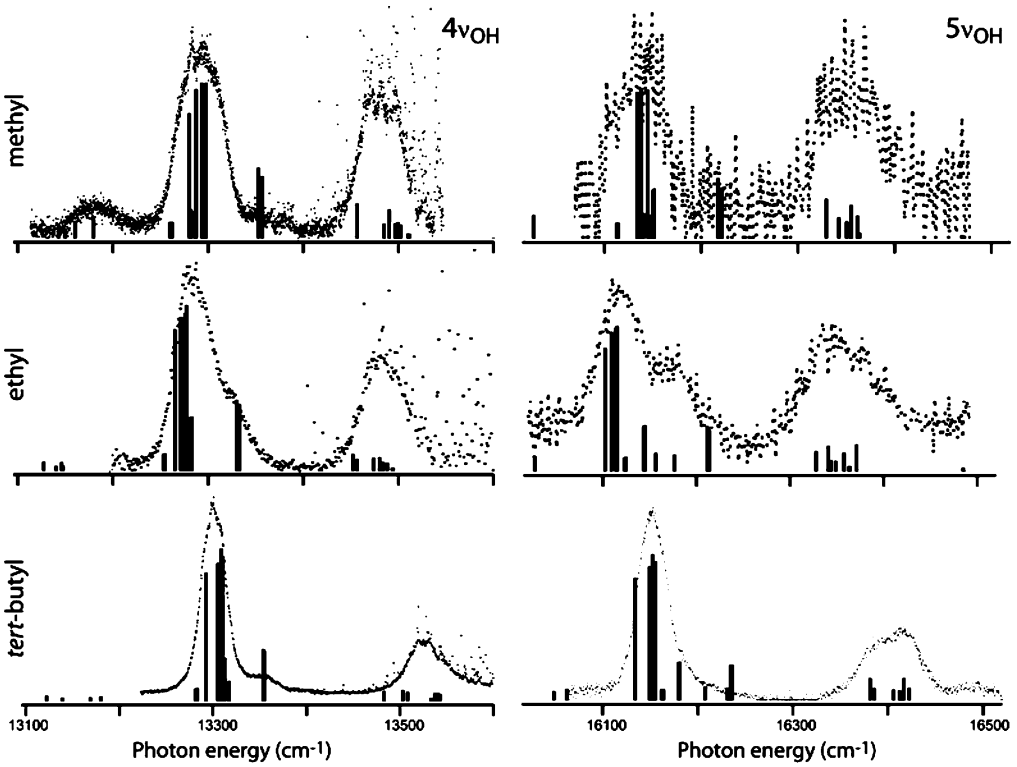

Figure 6. Simple stick simulations from the vibration−torsion model compared with experimental spectra of ROOH molecules. Input parameters for the model are listed in Tables 3 and 4. Scaling of simulated stick spectra to experimental spectra is arbitrary and meant for easy comparison of peak positions. Relative stick heights reflect Franck−Condon factors and relative initial populations only; predictions do not take into account the variation of the transition dipole moment with torsional angle.

enough (~152 cm^{-1}) that simulations no longer match experimental spectra. A low torsional barrier, such as that predicted for MeOOH, should have two predictable effects on O−H overtone spectra, both resulting from the population of torsionally excited states at room temperature. First, contributions from hot bands should be greater such that population of excited torsional states may account for the additional peak observed in MeOOH spectra at $4\nu_{OH}$ (Figure 3). Second, any dependence of the dipole moment function on torsional angle should become more pronounced since excited torsional states with energies near the top of the potential barrier have wave functions that spread to a wider range of torsional angles. For the case of MeOOH, therefore, calculations that address the dependence of the dipole moment function on torsional angle should show large changes in relative intensities from those in our current simulations.

In all three ROOH molecules the trans barrier to torsional motion about the O−O bond is lower than that in HOOH (387 cm^{-1} in the ground vibrational state[15]), a trend that is consistent with theoretical predictions.[36] As Likar et al.[4] note, Carpenter and Weinhold found that donation from a filled oxygen lone-pair in HOOH into an empty antibonding orbital (σ_{OH}*) on the opposite oxygen stabilizes the molecule at its equilibrium dihedral angle (111.83° [37]).[36] The relative stability at the energy minimum for HOOH increases its cis and trans barriers to torsional motion. The effect relies on the equilibrium dihedral angle being small enough to allow for good orbital overlap. Citing less overlap with the antibonding orbital in the case of *t*-BuOOH, Likar et al.[4] argue that *t*-BuOOH has less stabilization and therefore a lower trans barrier compared to HOOH. Indeed for the ROOH series studied here, the dihedral angles are larger (Table 3) and the barriers to torsion about the O−O bond are lower (Table 4) than those for HOOH. MeOOH, which has the largest dihedral angle (Table 3), also has the lowest torsional barrier (Table 4). This observed correlation between dihedral angle and torsional barrier height supports the effect proposed by Carpenter and Weinhold and suggests that the ground-state dihedral angle is a good predictor of relative barrier height in hydroperoxides (ROOH).[36]

5. Summary

Cross sections for overtone excitation of MeOOH, EtOOH, and *t*-BuOOH at $4\nu_{OH}$ and $5\nu_{OH}$ obtained by photoacoustic spectroscopy provide experimental values that may be useful for determining the relative importance of direct overtone photolysis of MeOOH and EtOOH at $5\nu_{OH}$ and $6\nu_{OH}$. To account theoretically for the integrated cross sections, modifications of the vibration−torsion model to account for the dipole moment dependence on torsional angle are currently underway.

The coarse features in the photoacoustic spectra can be accounted for by the vibration−torsion model of Crim and coworkers.[5] The vibration−torsion analysis and ab initio calculations imply a lower trans barrier to torsion about the O−O bond in MeOOH and EtOOH versus that in *t*-BuOOH, with a trend of increasing barrier height with increasing bulkiness of the R group and with decreasing torsional angle.

Future plans for the lab include a more thorough investigation of the absorption cross section of MeOOH at $5\nu_{OH}$ where direct overtone dissociation to produce OH radicals should become possible for states with high rotational energy. The lab is in the process of preparing for detection of OH radicals from overtone excitation of ROOH molecules.

Acknowledgment. Instrumental to this work were Charles Amass, Prof. R. B. Metz, Greg Young, and John Kosakowski, whom we thank for technical help, including assembly of the microphone apparatus. We are grateful to Prof. F. F. Crim for

giving us Dr. H-.R. Dübal's computer code (ROLFFAST) and to Prof. D. Bickar for helping with the MeOOH synthesis. S.H. thanks Prof. Crim, Prof. Metz, Dr. Steve S. Brown, Dr. Mac G. Brown, and Prof. R. G. Linck for scientific advice. Former Smith College students who assisted in building the lab include Christine Johnson, Kendra Beadle, and Katie Montgomery. We thank Lauren Grandpre and Lydia Morrison for assistance in collecting data. S.H. thanks Smith College and Research Corporation for funding (CC5623).

References and Notes

(1) Donaldson, D. J.; Frost, G. J.; Rosenlof, K. H.; Tuck, A. F.; Vaida, V. *Geophys. Res. Lett.* **1997**, *24*, 2651.

(2) Donaldson, D. J.; Tuck, A. F.; Vaida, V. *Chem. Rev.* **2003**, *103*, 4717.

(3) Finlayson-Pitts, B. J.; Pitts, J. N., Jr. *Chemistry of the Upper and Lower Atmosphere*; Academic Press: San Diego, CA, 2000.

(4) Likar, M. D.; Baggott, J. E.; Crim, F. F. *J. Chem. Phys.* **1989**, *90*, 6266.

(5) Dübal, H.-R.; Crim, F. F. *J. Chem. Phys.* **1985**, *83*, 3863.

(6) Roehl, C. M.; Nizkorodov, S. A.; Zhang, H.; Blake, G. A.; Wennberg, P. O. *J. Phys. Chem. A* **2002**, *106*, 3766.

(7) Bach, R. D.; Ayala, P. Y.; Schlegel, H. B. *J. Am. Chem. Soc.* **1996**, *118*, 12758.

(8) Rizzo, T. R.; Hayden, C. C.; Crim, F. F. *J. Chem. Phys.* **1984**, *81*, 4501.

(9) Rizzo, T. R.; Crim, F. F. *J. Chem. Phys.* **1982**, *76*, 2754.

(10) Chuang, M.-C.; Baggott, J. E.; Chandler, D. W.; Farneth, W. E.; Zare, R. N. *Faraday Discuss. Chem. Soc.* **1983**, *75*, 301.

(11) Chandler, D. W.; Farneth, W. E.; Zare, R. N. *J. Chem. Phys.* **1982**, *77*, 4447.

(12) Gai, H.; Thompson, D. L.; Fisk, G. A. *J. Chem. Phys.* **1989**, *90*, 7055.

(13) Brown, S. S.; Wilson, R. W.; Ravishankara, A. R. *J. Phys. Chem. A* **2000**, *104*, 4976.

(14) Tonmunphean, S.; Parasuk, V.; Karpfen, A. *J. Phys. Chem. A* **2002**, *106*, 438.

(15) Flaud, J.-M.; Camy-Peyret, C.; Johns, J. W. C.; Carli, B. *J. Chem. Phys.* **1989**, *91*, 1504.

(16) Tyblewski, M.; Ha, T.-K.; Meyer, R.; Bauder, A.; Blom, C. E. *J. Chem. Phys.* **1992**, *97*, 6168.

(17) August, J.; Brouard, M.; Docker, M. P.; Milne, C. J.; Simons, J. P.; Lavi, R.; Rosenwaks, S.; Schwartz-Lavi, D. *J. Phys. Chem.* **1988**, *92*, 5485.

(18) Bair, R. A.; Goddard, W. A., III *J. Am. Chem. Soc.* **1982**, *104*, 2719.

(19) Shin, S. K.; Park, S. O.; Choi, Y. S.; Kim, H. L.; Park, C. R. *J. Phys. Chem. A* **2001**, *105*, 10018.

(20) Davies, D. M.; Deary, M. E. *J. Chem. Soc., Perkin Trans. 2* **1992**, 559.

(21) We thank Brian Heikes for advice on the synthesis.

(22) Vaghjiani, G. L.; Ravishankara, A. R. *J. Phys. Chem.* **1989**, *93*, 1948.

(23) Behrman, E. J.; Biallas, M. J.; Brass, H. J.; Edwards, J. O.; Isaks, M. *J. Org. Chem.* **1970**, *35*, 3069.

(24) Sellers, R. M. *Analyst* (*London*) **1980**, *105*, 950.

(25) Gutow, J. H.; Davidsson, J.; Zare, R. N. *Chem. Phys. Lett.* **1991**, *185*, 120.

(26) Rothman, L. S.; Barbe, A.; Benner, D. C.; Brown, L. R.; Camy-Peyret, C.; Carleer, M. R.; Chance, K.; Clerbaux, C.; Dana, V.; Devi, V. M.; Fayt, A.; Flaud, J.-M.; Gamache, R. R.; Goldman, A.; Jacquemart, D.; Jucks, K. W.; Lafferty, W. J.; Mandin, J.-Y.; Massie, S. T.; Nemtchinov, V.; Newnham, D. A.; Perrin, A.; Rinsland, C. P.; Schroeder, J.; Smith, K. M.; Smith, M. A. H.; Tang, K.; Toth, R. A.; Vander Auwera, J.; Varanasi, P.; Yoshino, K. *J. Quant. Spectrosc. Radiat. Transfer* **2003**, *82*, 5.

(27) Homitsky, S. C. Honors Thesis, Smith College, 2004.

(28) Schumb, W. C.; Satterfield, C. N.; Wentworth, R. L. *Hydrogen Peroxide*; Reinhold Publishing Corporation: New York, 1955.

(29) O'Sullivan, D. W.; Lee, M. H.; Noone, B. C.; Heikes, B. G. *J. Phys. Chem.* **1996**, *100*, 3241.

(30) Lee, M.; Heikes, B. G.; O'Sullivan, D. W. *Atmos. Environ.* **2000**, *34*, 3475.

(31) Bergeat, A.; Cavagnat, D.; Lapouge, C.; Lespade, L. *J. Phys. Chem. A* **2000**, *104*, 9233.

(32) Rong, Z.; Kjaergaard, H. G. *J. Phys. Chem. A* **2002**, *106*, 6242.

(33) Zhu, C.; Kjaergaard, H. G.; Henry, B. R. *J. Chem. Phys.* **1997**, *107*, 691.

(34) Frisch, M. J.; Trucks, G. W.; Schlegel, H. B.; Scuseria, G. E.; Robb, M. A.; Cheeseman, J. R.; Zakrewski, V. G.; Montgomery, J. A., Jr.; Stratmann, R. E.; Burant, J. C.; Dapprich, S.; Millam, J. M.; Daniels, A. D.; Kudin, K. N.; Strain, M. C.; Farkas, O.; Tomasi, J.; Barone, V.; Cossi, M.; Cammi, R.; Mennucci, B.; Pomelli, C.; Adamo, C.; Clifford, S.; Ochterski, J.; Petersson, G. A.; Ayala, P. Y.; Cui, Q.; Morokuma, K.; Malick, D. K.; Rabuck, A.; Raghavachari, K.; Foresman, J. B.; Cioslowski, J.; Ortiz, J. V.; Stefanov, B. B.; Liu, G.; Liashenko, A.; Piskorz, P.; Komaromi, I.; Comperts, R.; Martin, R. L.; Fox, D. J.; Keith, T.; Al-Laham, M. A.; Peng, C. Y.; Nanayakkara, A.; Gonzales, C.; Challacombe, M.; Gill, P. M. W.; Johnson, B. G.; Chen, W.; Wong, M. W.; Andres, J. L.; Head-Gordon, M.; Replogle, E. S.; Pople, J. A. *Gaussian 98*, revision A.6; Gaussian, Inc.: Pittsburgh, PA, 1998.

(35) Quack, M. *Annu. Rev. Phys. Chem.* **1990**, *41*, 839.

(36) Carpenter, J. E.; Weinhold, F. *J. Phys. Chem.* **1988**, *92*, 4306.

(37) Cremer, D. *J. Chem. Phys.* **1978**, *69*, 4440.